Current Biology, Vol. 13, 1488–1498, September 2, 2003, ©2003 Elsevier Science Ltd. All rights reserved. DOI 10.1016/S0960-9822(03)00582-7

TAC-1 and ZYG-9 Form a Complex that Promotes Microtubule Assembly in *C. elegans* Embryos

Jean-Michel Bellanger and Pierre Gönczy*
Swiss Institute for Experimental Cancer Research (ISREC)
CH-1066 Epalinges/Lausanne
Switzerland

Summary

Background: Modulation of microtubule dynamics is crucial for proper cell division. While a large body of work has made important contributions to our understanding of the mechanisms governing microtubule dynamics in vitro, much remains to be learned about how these mechanisms operate in vivo.
Results: We identified TAC-1 as the sole TACC (Transforming Acidic Coiled Coil) protein in *C. elegans*. TAC-1 consists essentially of a TACC domain, in contrast to the much larger members of this protein family in other species. We find that *tac-1* is essential for pronuclear migration and spindle elongation in one-cell-stage *C. elegans* embryos. Using an in vivo FRAP-based assay, we establish that inactivation of *tac-1* results in defective microtubule assembly. TAC-1 is present in the cytoplasm and is enriched at centrosomes in a cell cycle-dependent manner. Centrosomal localization is independent of microtubules but requires the activity of γ-tubulin and the Aurora-A kinase AIR-1. By conducting FRAP analysis in embryos expressing GFP-TAC-1, we find that centrosomal TAC-1 exchanges rapidly with the cytoplasmic pool. Importantly, we establish that TAC-1 physically interacts with ZYG-9, a microtubule-associated protein (MAP) of the XMAP215 family, both in vitro and in vivo. Furthermore, we also uncover that TAC-1 and ZYG-9 stabilize each other in *C. elegans* embryos.
Conclusions: Our findings identify TAC-1 as a core structural and functional member of the evolutionarily conserved TACC family of proteins and suggest that mutual stabilization between TACC and XMAP215 proteins is a key feature ensuring microtubule assembly in vivo.

Introduction

Microtubules are polar structures that, in most animal cells, are nucleated from centrosomes, where their minus end is located, and that grow primarily through polymerization at their plus end. Microtubules exhibit dynamic instability, alternating between periods of growth and shrinkage [1]. This is thought to be important notably for capture of binding sites at kinetochores and at the cell cortex; this capture thus permits correct chromosome segregation and spindle positioning [2].

Microtubule dynamics are modulated by a number of MAPs. *Xenopus laevis* XMAP215 is a particularly important MAP that was discovered as an activity promoting microtubule polymerization at plus ends and turned out to be a major factor ensuring microtubule growth throughout the cell cycle [3–5]. Homologs of XMAP215 are present in all eukaryotes, including *H. sapiens* (ch-TOG), *D. melanogaster* (Msps), and *C. elegans* (ZYG-9) (see [6] for a review). Inactivation of XMAP215 family members typically results in short microtubules and aberrant spindle assembly, although whether this is due to impaired growth at the plus ends has not been determined in vivo [7–10]. Intriguingly, members of the XMAP215 protein family are enriched at centrosomes and spindle poles, rather than at the plus ends of microtubules. Recent evidence indicates that XMAP215 can also promote microtubule depolymerization in *Xenopus* egg extracts [11]. Although this activity appears to be specific to plus ends, it has been suggested that XMAP215 at centrosomes may help depolymerize microtubules that are misoriented with their minus end facing out [11].

Work in *Drosophila* has led to the identification of D-TACC (Transforming and Acidic Coiled-Coil) as a key regulator of Msps function [12, 13]. D-TACC is enriched at centrosomes and physically interacts with Msps. Moreover, Msps enrichment at centrosomes is diminished when D-TACC levels are reduced [12]. These findings have led to the proposal that D-TACC plays a crucial role in recruiting or maintaining Msps at centrosomes and thus helps it bind to microtubule plus ends as they grow out from centrosomes. Compatible with this model, imaging of D-TACC-GFP and Msps-GFP revealed small dots oscillating to and from the centrosomes [12]. Whether a requirement for TACC proteins in recruiting or maintaining XMAP215 family members at centrosomes is evolutionarily conserved, or whether D-TACC may play a more general role in Msps metabolism, remains to be clarified.

The early *C. elegans* embryo is particularly well suited for a high-resolution analysis of the spatial and temporal control of microtubule dynamics in living organisms. As is the case for other eukaryotes, the *C. elegans* XMAP215 family member ZYG-9 is required for microtubule-dependent processes: embryos derived from mothers lacking *zyg-9* function have short astral microtubules and fail to undergo microtubule-dependent processes such as pronuclear migration and spindle elongation [7, 14]. ZYG-9 is enriched at centrosomes, but it is also present to a significant extent in the cytoplasm [14]. Whether a TACC protein may modulate ZYG-9 function has not been established to date.

Results

TAC-1, the Sole TACC Protein Family Member of *C. elegans*

We have previously identified the MAP ZYG-8 as being required for microtubule stabilization during anaphase in *C. elegans* embryos [15]. In the course of a screen aimed at uncovering molecular partners of ZYG-8, we

*Correspondence: pierre.gonczy@isrec.unil.ch

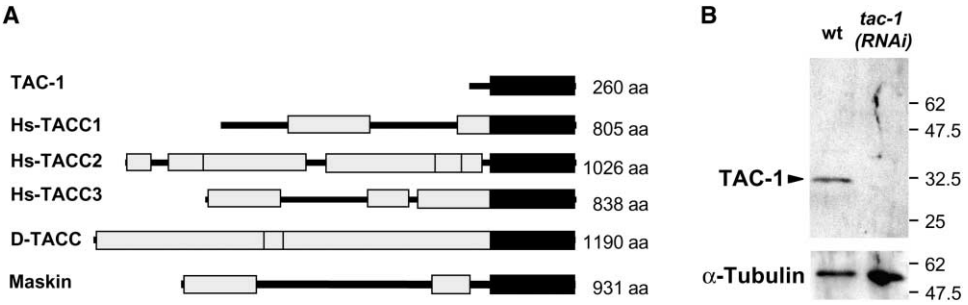

Figure 1. *C. elegans tac-1* Encodes a 260 Amino Acid TACC Protein

(A) The domain structure of TACC proteins (Prodom Release 2001.3). The conserved TACC domain is depicted in black, and other protein-specific domains are depicted as gray boxes.

(B) A Western blot of wild-type and *tac-1(RNAi)* embryonic extracts probed with anti-TAC-1 antibodies and reprobed with anti-α-tubulin antibodies. The numbers on the right represent molecular weight markers (in kDa).

isolated the product of the *tac-1* gene (see the Experimental Procedures). The analysis of the interaction between ZYG-8 and TAC-1 will be discussed elsewhere. Here, we report our findings on the function of TAC-1 during early *C. elegans* embryogenesis.

We determined that *tac-1* consists of three exons *trans* spliced to the SL1 leader sequence; this complex generates a single 800 base pair RT-PCR species (see Figures S1A and S1B in the Supplemental Data available with this article online). *tac-1* is predicted to encode a 260 amino acid polypeptide that consists essentially of a coiled-coil domain characteristic of TACC (Transforming and Acidic Coiled-Coil) proteins (Figures 1A and S1C [in the Supplemental Data]). We raised antibodies against TAC-1 that recognize a single band of the expected molecular weight (~30 kDa) in wild-type embryonic extracts; however, this band is not detectable in *tac-1(RNAi)* embryonic extracts (Figure 1B). Owing to the presence of divergent N-terminal domains, members of the TACC protein family in other species are much larger than TAC-1 (Figure 1A and [16]). However, Blast searches of the complete *C. elegans* genome sequence did not reveal any other TACC domain-containing protein.

Taken together, these findings establish that TAC-1 consists essentially of a TACC domain and is the sole TACC protein in *C. elegans*.

tac-1 Is Required for Pronuclear Migration and Spindle Elongation

We investigated the consequence of inactivating *tac-1* by using dual DIC and fluorescence time-lapse microscopy of one-cell-stage embryos expressing GFP-β-tubulin (GFP-TUB) and GFP-histone2B (GFP-HIS) to simultaneously follow centrosomes and chromosomes.

In wild-type (Figure 2A and Movie 1 in the Supplemental Data), the female and male pronuclei become visible shortly after the completion of meiosis. The female pronucleus is located at the anterior, and the male pronucleus and associated centrosomes are located at the posterior (Figure 2A, 00:00). Pronuclear migration ensues. After meeting in the posterior of the embryo (Figure 2A, 02:00), the pronuclei and associated centrosomes move to the cell center while undergoing a 90° rotation. As a result, the bipolar spindle assembles in the cell center and along the anterior-posterior (AP) axis (Figure 2A, 06:30). During anaphase, the spindle elongates asymmetrically toward the posterior, leading to an unequal first cleavage (Figure 2A, 08:30).

In most (22/24) *tac-1(RNAi)* embryos (Figure 2B and Movie 2 in the Supplemental Data), there is one female and one male pronucleus that become visible in their characteristic locations (Figure 2B, 00:00). However, the size of the polar bodies is sometimes abnormal (data not shown), and in rare cases (2/24), two or more female pronuclei are observed, indicating that *tac-1* plays some role during the meiotic divisions. Strikingly, we found that pronuclear migration fails in all *tac-1(RNAi)* embryos (Figure 2B, 01:50). As a result, the bipolar spindle assembles in the cell posterior and is orthogonal to the AP axis (Figure 2B, 05:40). Moreover, the metaphase spindle is significantly shorter than in wild-type embryos (compare Figures 2A, 06:30 and 2B, 05:40, 9.7 ± 0.5 μm instead of 13.4 ± 0.8 μm) and hardly elongates during anaphase (compare Figures 2A, 08:30 and 2B, 07:50, 12.2 ± 0.9 μm instead of 21 ± 1.1 μm in wild-type). This is unlikely to be due merely to geometric constraints conferred by the eggshell, as the spindle can elongate in other cases when the spindle sets up transverse to the AP axis (e.g., [17]). Astral microtubule arrays are also dramatically reduced in *tac-1(RNAi)* embryos (compare, for instance, Figures 3C and 3E). As anticipated from such defects, the first cleavage is aberrant, and *tac-1(RNAi)* results in fully penetrant embryonic lethality. We conclude that *tac-1* is required for pronuclear migration and spindle elongation in one-cell-stage *C. elegans* embryos.

FRAP-Based Assay Reveals that *tac-1* Promotes Microtubule Assembly

We next sought to assay the requirement of TAC-1 for microtubule assembly in real time. To this end, we designed a fluorescence recovery after photobleaching (FRAP)-based assay to measure the overall assembly rate of a population of microtubules by using GFP-TUB transgenic embryos. We photobleached a ~3–4 μm square centered on one of the asters in late prometaphase/early metaphase of wild-type and *tac-1(RNAi)* one-cell-stage embryos. We used time-lapse confocal microscopy to assay subsequent fluorescence recovery in two areas: a disc ~2 μm in diameter corresponding

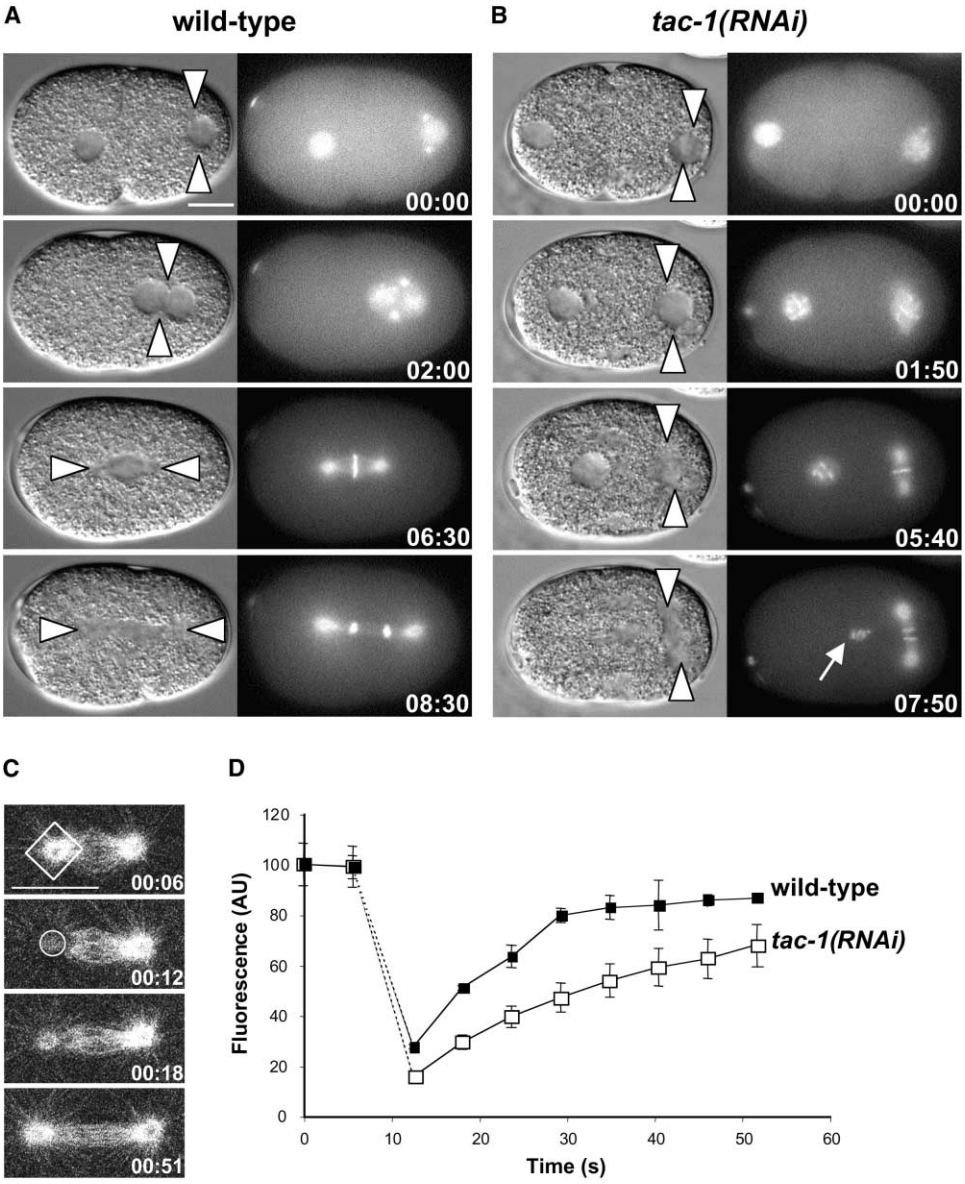

Figure 2. *tac-1* Is Required for Pronuclear Migration and Spindle Elongation and Promotes Microtubule Assembly in One-Cell-Stage *C. elegans* Embryos

(A and B) Images from dual DIC and fluorescence microscopy time-lapse sequences of (A) wild-type and (B) *tac-1(RNAi)* one-cell-stage embryos expressing GFP-TUB and GFP-HIS (see also corresponding Movies 1 and 2 [see the Supplemental Data]). In this and other figures, anterior is oriented toward the left, and posterior is oriented toward the right. The scale bars represent 10 μm, and all panels within a figure are at approximately the same magnification, unless otherwise stated. Time elapsed is shown in minutes and seconds, with 00:00 corresponding to the time of maximal pseudocleavage furrow ingression. The arrowheads point to centrosomes (one is out of focus in *tac-1(RNAi)* at time 00:00) and spindle poles. Pronuclear migration does not take place in *tac-1(RNAi)* embryos ([B], 01:50), and a short spindle assembles orthogonally to the AP axis in the cell posterior ([B], 05:40). Note that chromosomes from the female pronucleus ([B], 07:50, arrow) are drawn toward the spindle after nuclear envelope breakdown.

(C) Images from a confocal time-lapse sequence of a wild-type embryo expressing GFP-TUB. Photobleaching of an ~3–4 μm square (indicated in white) started at time 00:06 and ended at time 00:075. Recovery was assessed within the square, and the disc is represented at time 00:12 (see text).

(D) A plot of FRAP experiments with GFP-TUB. Recovery of fluorescence intensity (intensities in square minus intensities in disc) was determined over the indicated time. Black squares, wild-type; white squares, *tac-1(RNAi)*. Averages of three (wild-type) and seven (*tac-1(RNAi)*) experiments are shown along with standard deviations. AU, arbitrary units.

to the centrosome and the square corresponding to the bleached area (Figure 2C). We substracted the values obtained in the circle from those obtained in the square to limit the impact of microtubule nucleation on the measurements. As illustrated in Figure 2D, these measurements showed that the initial recovery of fluorescence occurs at a rate of 4.2% ± 0.02% per second in wild-type, compared to 2.4% ± 0.2% per second in *tac-*

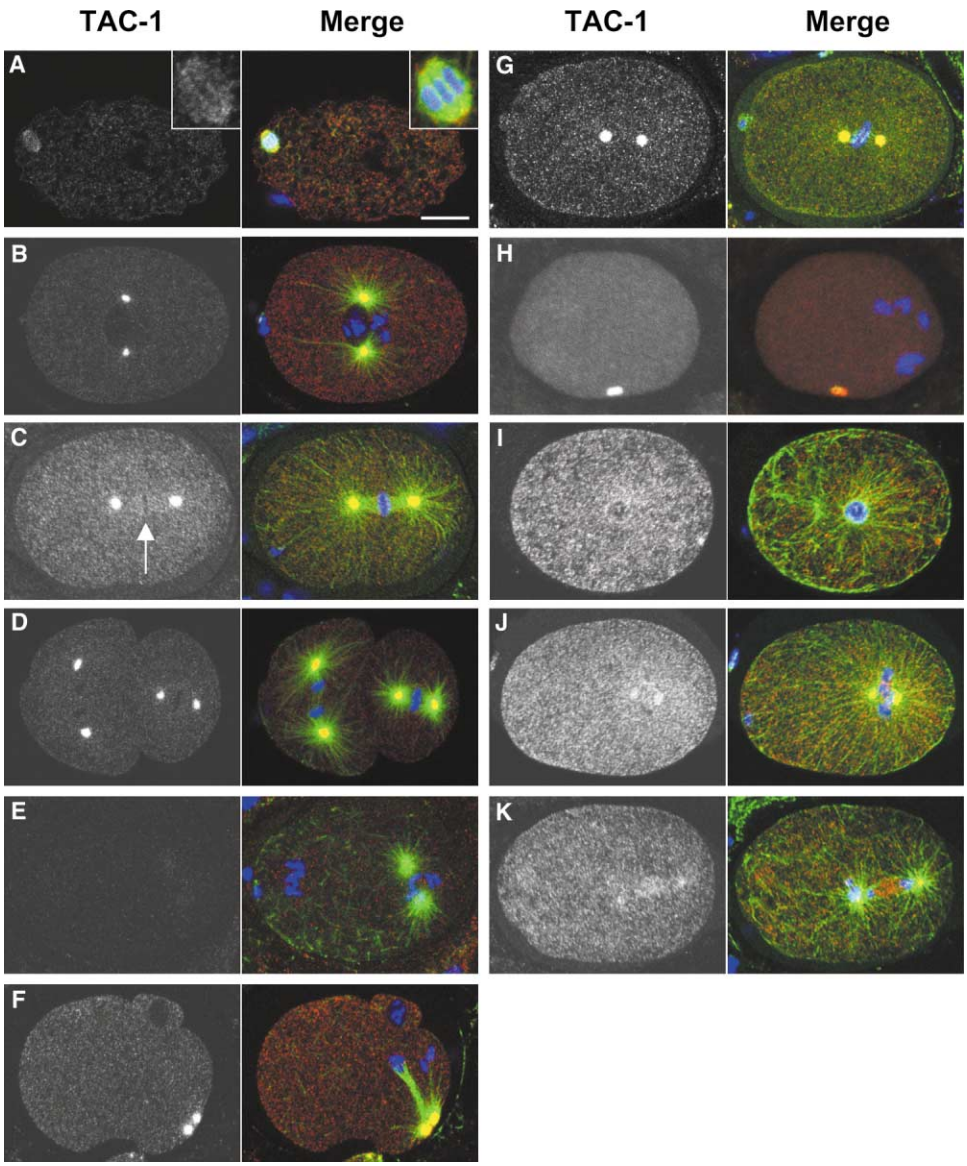

Figure 3. TAC-1 Is Present in the Cytoplasm and at Centrosomes

(A–K) One-cell-stage embryos stained with antibodies against TAC-1 and α-tubulin. The panels on the left show anti-TAC-1 staining, and the panels on the right show a merge of TAC-1 (red), α-tubulin (green), and Hoechst counterstain to view DNA (blue). (A–D) Wild-type. TAC-1 is slightly enriched at spindle poles during the (A) meiotic division, and more so at centrosomes in one-cell-stage embryos during (B) prophase and thereafter (C and D) during the cell cycle. Moreover, TAC-1 is present in the cytoplasm throughout the cell cycle. Note weak enrichment on the spindle during metaphase (C), particularly in the vicinity of the chromosomes (arrow). (E) *tac-1(RNAi)*, prometaphase. Both centrosomal and cytoplamic signals are essentially absent. (F–H) (F) *dhc-1(RNAi*), mitosis; (G) cold-treated, metaphase; (H) *tba-2(RNAi)*, mitosis. In all three cases, TAC-1 distribution is as in wild-type. (I) *spd-5(or213)*. Although TAC-1 is not enriched in a structure that resembles centrosomes, note the weak enrichment around the chromosomes. (J) *tbg-1(t1465)*, metaphase equivalent. Centrosomal TAC-1 is diminished. (K) *air-1(RNAi)*, anaphase equivalent. The TAC-1 signal at spindle poles is minimal. Note also the slight enrichment between the spindle poles.

1(RNAi) embryos (see the Experimental Procedures). These findings establish that *tac-1* promotes overall microtubule assembly in living *C. elegans* embryos.

TAC-1 Distribution

We next sought to determine the subcellular distribution of TAC-1. Using affinity-purified antibodies, we found that TAC-1 is slightly enriched at spindle poles during the meiotic division (Figure 3A). We observed a more significant enrichment of TAC-1 at centrosomes in one-cell-stage embryos during prophase (Figure 3B); the intensity of this centrosomal signal increases further throughout mitosis, and culminates in anaphase (Figures 3C and 3D). During metaphase, TAC-1 is also weakly enriched on the spindle, particularly in the vicinity of chromosomes (Figure 3C, arrow). This finding is consistent with the notion that TAC-1 may be enriched at the plus end of microtubules. In addition, we found that TAC-1 is present in the cytoplasm of early embryos throughout the cell cycle (Figures 3A–3D). Both centro-

somal and cytoplasmic signals are essentially absent in *tac-1(RNAi)* embryos (Figure 3E); the absence of these signals confirms that they correspond to bona fide TAC-1 distribution.

We then investigated the mechanisms of TAC-1 recruitment to centrosomes. We first tested whether centrosomal localization is mediated by the minus end-directed motor cytoplasmic dynein [18]. However, we found that TAC-1 distribution is not affected in embryos in which the dynein heavy chain *dhc-1* has been inactivated by RNAi (Figure 3F). We found the same to be true when microtubules are depolymerized by cold treatment (Figure 3G). Furthermore, TAC-1 is still enriched at centrosomes in embryos that have always been devoid of microtubules due to RNAi of the α-tubulin gene *tba-2* (Figure 3H). Interestingly, the intensity of centrosomal TAC-1 still increases throughout mitosis in such embryos (data not shown). Therefore, microtubules are not required for either the recruitment, the maintenance, or the cell cycle-dependent increase of centrosomal TAC-1. Taken together, these findings establish that TAC-1 is a core component of centrosomes in *C. elegans*.

We next tested which other centrosomal components may control TAC-1 distribution. We first investigated embryos lacking the function of *spd-5*, which encodes a coiled-coil protein required for an initial step in centrosome maturation [19]. In *spd-5(or213)* mutant embryos, no functional centrosome is assembled and microtubules are organized instead around chromosomes. As expected, we found that TAC-1 is no longer enriched in discrete subcellular locations in *spd-5(or213)* mutant embryos (Figure 3I). We then tested whether centrosomal TAC-1 is affected in embryos lacking the function of γ-tubulin or of the Aurora-A kinase AIR-1, which are both required for a later step in centrosome maturation [20–22]. We observed that centrosomal accumulation of TAC-1 was markedly diminished in *tbg-1(t1465)* mutant embryos (Figure 3J), and even more so in *air-1(RNAi)* embryos (Figure 3K). This finding indicates that γ-tubulin and AIR-1 are both required for efficient recruitment and/or maintenance of TAC-1 at centrosomes.

TAC-1 Dynamics in Living Embryos

We generated a transgenic line expressing a fusion protein between GFP and TAC-1 to analyze distribution dynamics in living embryos. Time-lapse spinning-disc confocal microscopy demonstrates that GFP-TAC-1 is distributed in a manner essentially indistinguishable from endogenous TAC-1, as detected by our antibody (Movie 3 in the Supplemental Data).

To determine the dynamics of TAC-1 recruitment to centrosomes, we performed FRAP experiments with GFP-TAC-1 transgenic embryos. We photobleached one centrosome in one-cell-stage embryos during prophase and assayed subsequent fluorescence recovery by using four-dimensional confocal microscopy (Experimental Procedures). Strikingly, we found that the GFP signal at the centrosome recovers very rapidly (Figures 4A and 4B; $t_{1/2} \approx 25$ s). Moreover, the bulk of the signal recovers, indicating that the vast majority of centrosomal TAC-1 is mobile (Figure 4B). We found similar results for embryos during metaphase, while recovery is much less pronounced for embryos during anaphase (data not shown). We conclude that TAC-1 at centrosomes can rapidly exchange with the cytoplasmic protein pool.

TAC-1 Physically Interacts with ZYG-9 both In Vitro and In Vivo

The *tac-1(RNAi)* phenotype is indistinguishable from that of *zyg-9* mutant embryos, and TAC-1, like ZYG-9, is present in the cytoplasm and is enriched at centrosomes [14]. These observations raise the possibility that TAC-1 and ZYG-9 interact and function together in *C. elegans* embryos. Compatible with a physical association, embryos simultaneously stained with anti-TAC-1 and anti-ZYG-9 antibodies exhibit tight colocalization of the two proteins at centrosomes throughout the cell cycle (Figure S2A [in the Supplemental Data] and data not shown).

We used a GST pull-down assay to directly probe the interaction between TAC-1 and ZYG-9. As shown in Figure 5A, we found that GST-TAC-1, but not GST alone, efficiently retains in vitro-translated ZYG-9. We used the GST pull-down assay to map the domains within ZYG-9 that mediate interaction with TAC-1, and we found them to lie within three segments (amino acids 654–937, 908–1167, and 1162–1415) located in the C-terminal half of the protein (Figure 5B). We found that TAC-1 and fragments of ZYG-9 also bind to each other in yeast two-hybrid screens (data not shown); these data confirm that TAC-1 and ZYG-9 can physically interact.

We next aimed at determining if TAC-1 and ZYG-9 also associate in *C. elegans* embryos. To this end, we performed immunoprecipitation (Ip) experiments from embryonic extracts by using antibodies against TAC-1, ZYG-9, or GFP as a negative control, followed by Western blot analysis of the resulting immunocomplexes. As shown in Figure 5C, we found that TAC-1 and ZYG-9 are efficiently immunoprecipitated from the extract by their own antibodies. We found, in addition, that substantial amounts of TAC-1 are coimmunoprecipitated by anti-ZYG-9 antibodies and, conversely, that substantial amounts of ZYG-9 are coimmunoprecipitated by anti-TAC-1 antibodies (Figure 5C). Because ZYG-9 is a MAP, we tested whether the interaction between TAC-1 and ZYG-9 is mediated by microtubules. However, we found that α-tubulin is not detected in these immunocomplexes (Figure 5C); this indicates that the two proteins do not associate in vivo through a microtubule interface. Taken together, these findings demonstrate that TAC-1 and ZYG-9 associate in *C. elegans* embryos.

To estimate the fractions of TAC-1 and ZYG-9 that participate in the TAC-1/ZYG-9 complex in vivo, we analyzed the fraction of each protein remaining in the extract after Ip. Quantification of the gel shown in Figure 5D indicates that Ip with the anti-ZYG-9 antibodies depleted the extract of $\sim$100% of ZYG-9 and $\sim$70% of TAC-1. Conversely, Ip with the anti-TAC-1 antibodies depleted the extract of $\sim$70% of TAC-1 and $\sim$90% of ZYG-9 (Figure 5D). While a more complete analysis must be performed to precisely quantify the fraction of each protein present in the complex, these initial rough estimates suggest that, in vivo, $\sim$70% of TAC-1 is associated with ZYG-9 and $\sim$90% of ZYG-9 is associated with TAC-1.

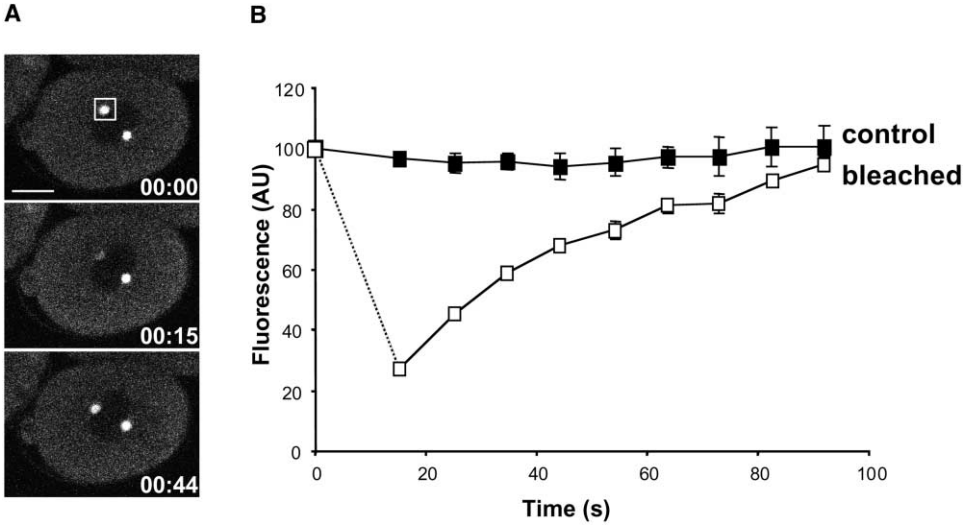

Figure 4. GFP-TAC-1 Dynamics in Living Embryos

(A) Images show select central focal planes from Figure 4D confocal time-lapse sequences. Photobleaching started within the indicated square at time 00:00 and ended at time 00:05. Note the rapid recovery of fluorescence at the targeted centrosome.

(B) A plot of FRAP experiments. Full projections of seven confocal slices taken ~1 μm apart were generated, and fluorescence intensity was determined for both centrosomes over the indicated time (which correspond to the end of stack acquisition). Black squares, control centrosome; white squares, photobleached centrosome. On the *y*-axis, 100% corresponds to the fluorescence intensity before photobleaching. The averages of five experiments are shown along with standard deviations (barely visible in some cases because of being very small); similar values were found by imaging a larger number of embryos in a single confocal plane (not shown). $t_{1/2}$ of recovery is ≈25 s. AU, arbitrary units.

TAC-1 and ZYG-9 Stabilize Each Other in *C. elegans* Embryos

We next investigated the mutual relationship of TAC-1 and ZYG-9. We first determined if *tac-1* is involved in the centrosomal recruitment of ZYG-9. We observed that ZYG-9 distribution at centrosomes is markedly reduced in the vast majority of *tac-1(RNAi)* embryos as compared to wild-type (Figures 6A and 6B). Unexpect-

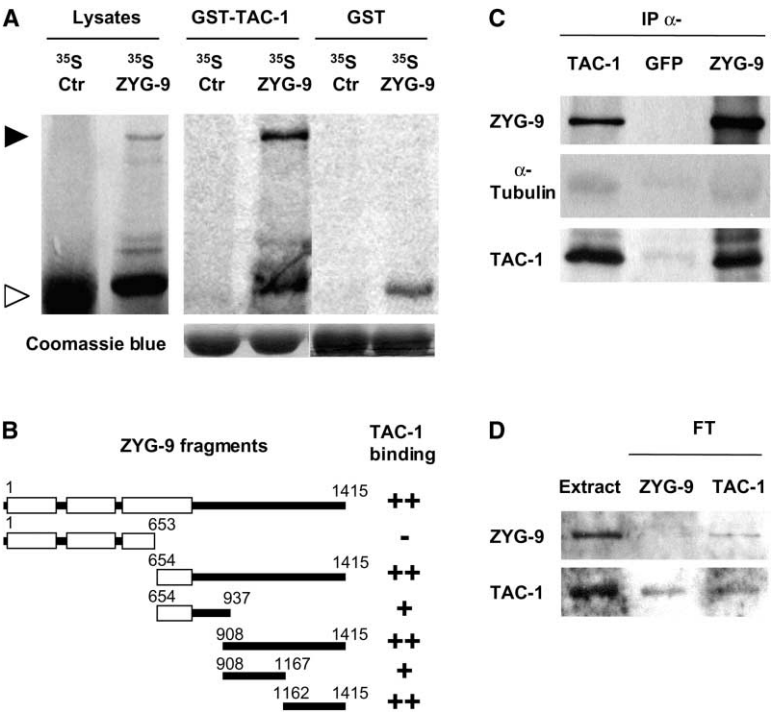

Figure 5. TAC-1 Physically Interacts with ZYG-9 Both In Vitro and In Vivo

(A) A GST pull-down assay. In vitro-translated, [^{35}S]-labeled ZYG-9 and control protein incubated with 10 μg GST-TAC-1 or GST, which are visualized by Coomassie Blue staining in the lower panel. Retained proteins are subjected to SDS-PAGE and are revealed by autoradiography. A fraction of the in vitro-translated species is loaded on the same gel to distinguish full-length ZYG-9 (black arrowhead) from a smaller and more abundant by-product (white arrowhead). GST-TAC-1, but not GST, retained full-length ZYG-9, while neither the shorter ZYG-9 by-product nor the control protein were specifically retained.

(B) A summary of GST pull-down experiments mapping the domains within ZYG-9 that interact with TAC-1. −, no interaction; +, interaction; ++, strong interaction. Note that three nonoverlapping segments within the C-terminal half of the protein can mediate interaction with TAC-1.

(C) Coimmunoprecipitation experiments. TAC-1, ZYG-9, and GFP (negative control) are independently immunoprecipitated from embryonic extracts, and the presence of TAC-1, ZYG-9, as well as that of α-tubulin in each immunocomplex is revealed by Western blot analysis. Note that TAC-1 and ZYG-9 coimmunoprecipitate when using either anti-TAC-1 or anti-ZYG-9 antibodies and that α-tubulin is not present in the immunocomplexes.

(D) Fractions of TAC-1 and ZYG-9 proteins remaining in the flow-through (FT) after immunoprecipitation (Ip), as revealed by Western blot analysis.

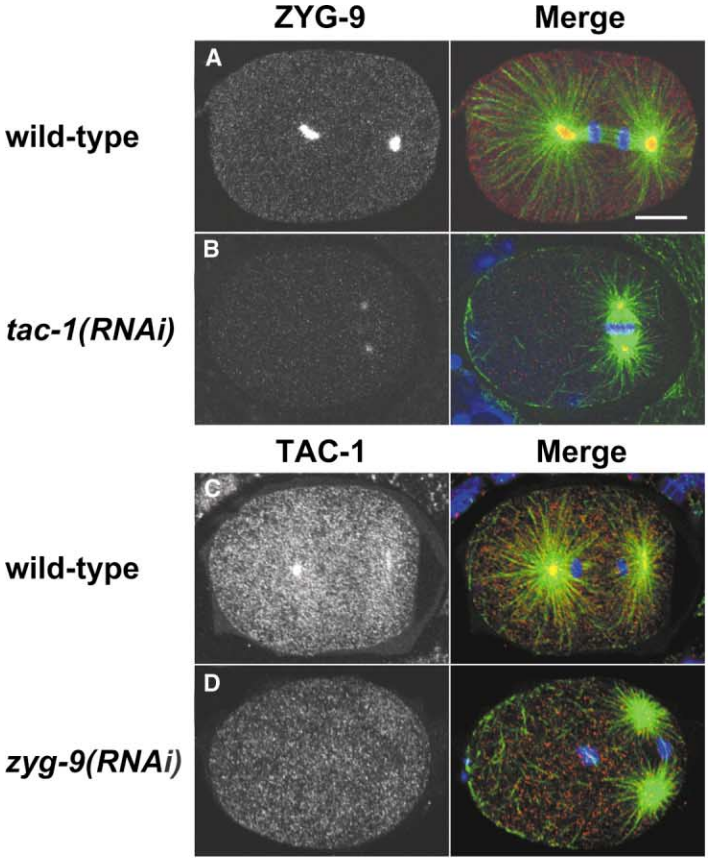
ZYG-9
Merge
A
wild-type
B
tac-1(RNAi)
TAC-1
Merge
C
wild-type
D
zyg-9(RNAi)

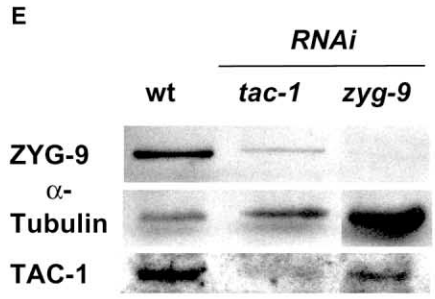
E
RNAi
wt
tac-1
zyg-9
ZYG-9
α-
Tubulin
TAC-1

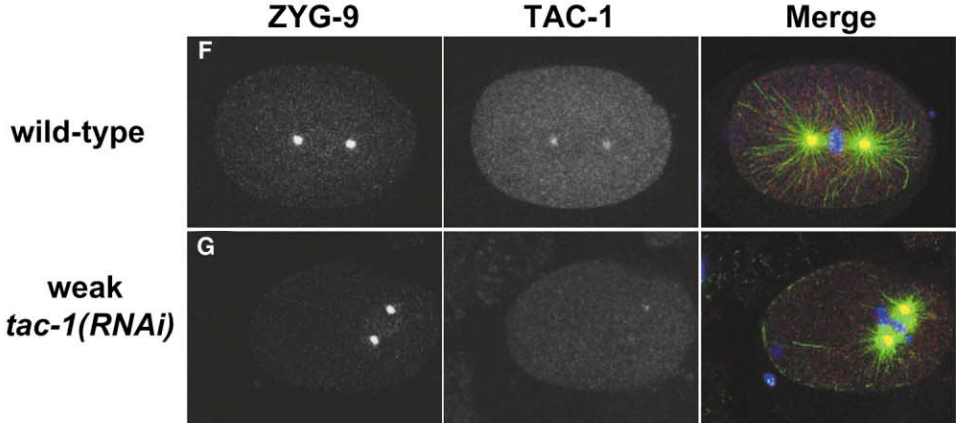
ZYG-9
TAC-1
Merge
F
wild-type
G
weak
tac-1(RNAi)

edly, we noticed, in addition, a striking reduction of the cytoplasmic signal (Figures 6A and 6B), suggesting that *tac-1* function controls the overall level of ZYG-9. To test this hypothesis further, we performed Western blot analysis of embryonic extracts prepared from wild-type and *tac-1(RNAi)* animals. Consistent with the immunostainings, we observed a severe reduction of the ZYG-9 signal in the *tac-1(RNAi)* embryonic extract (~10% of wild-type levels left; Figure 6E). We then determined if, conversely, *zyg-9* is required for centrosomal recruitment and normal protein levels of TAC-1. Again, we found that TAC-1 signals at centrosomes and in the cytoplasm are markedly reduced in *zyg-9(RNAi)* (Figure 6D) as compared to wild-type (Figure 6C); this finding is confirmed by Western blot analysis (~10% of wild-type levels left; Figure 6E). An identical conclusion was reached from immunostaining of *zyg-9(b244)* and *zyg-9(b279)* mutant embryos (Figure S2B in the Supplemental Data). Taken together, these observations establish that TAC-1 and ZYG-9 stabilize each other in *C. elegans* embryos. This is unlikely to reflect a general mechanism controlling centrosomal components since neither the centrosomal localization nor the overall protein level of γ-tubulin is affected by inactivation of *tac-1* or *zyg-9* (data not shown).

In the process of examining ZYG-9 distribution in *tac-1(RNAi)* embryos, we noticed rare embryos that exhibit diminished levels of ZYG-9 in the cytoplasm, but a signal at centrosomes indistinguishable from wild-type (compare Figures 6F and 6G). Such rare embryos have experienced incomplete *tac-1* inactivation (see Figure 6G, TAC-1 panel), yet they have set up a spindle orthogonal to the AP axis, indicative of a strong phenotype (compare Figure 6G with Figure 3E). These observations indicate that cytoplasmic ZYG-9 is most sensitive to the absence of *tac-1* function. Moreover, they suggest that having normal amounts of ZYG-9 at centrosomes is not sufficient for proper modulation of microtubule dynamics in early *C. elegans* embryos.

Discussion

TAC-1 Is a Core Structural and Functional TACC Protein

Transforming and Acidic Coiled-Coil (TACC) proteins have been identified initially in *H. sapiens*, where they have been postulated to contribute to cancer progression (see [23] for a review). All three human TACC proteins, as well as D-TACC and the related *Xenopus* Maskin, are fairly large, ranging from 805 to 1190 amino acids in size and having in common only an ~200 amino acid TACC domain located in the C terminus [16]. Despite this overall structural heterogeneity, all five proteins are enriched at centrosomes, albeit to different extents and at different moments of the cell cycle. Moreover, the TACC domain of D-TACC is sufficient for centrosomal targeting [24]. Whether the TACC domain of other family members can do the same and whether the TACC domain of D-TACC is also sufficient for function has not been established.

We identified TAC-1 as the sole TACC protein in *C. elegans*. Unexpectedly, given the structure of family members in other species, TAC-1 is a short protein that consists essentially of a TACC domain. TAC-1 is enriched on centrosomes and functions to promote microtubule assembly. Therefore, the TACC domain alone is sufficient not only for centrosomal targeting, but can also be sufficient for function. It is possible that a common family ancestor also consisted essentially of a TACC domain, with protein-specific N-terminal domains having been added subsequently in other species. Overall, TAC-1 represents a structural and functional core whose analysis is expected to yield unique insights into the function of all TACC proteins.

Centrosomal TAC-1 Rapidly Exchanges with a Cytoplasmic Pool

While TACC proteins are enriched at centrosomes, all three human TACC proteins as well as D-TACC are also clearly present in the cytoplasm [25]. Similarly, a substantial fraction of TAC-1 is cytoplasmic in early *C. elegans* embryos. In *Drosophila*, FRAP experiments have led to the conclusion that centrosomal D-TACC cycles relatively slowly ($t_{1/2} \approx 2$ min) [26]. However, these experiments were conducted by bleaching large areas that contain several centrosomes and surrounding cytoplasm; thus, the exchange rate between centrosomal and cytoplasmic pools was not directly assessed. In contrast, we tested specifically the dynamics of centrosomal GFP-TAC-1 in *C. elegans* with high spatial resolution. We discovered that the bulk of centrosomal TAC-1 undergoes rapid exchange with the cytoplasmic pool ($t_{1/2} \approx 25$ s). Such a rapid turnover raises the possibility that TACC proteins may merely transit through centrosomes to become modified or associated with partner proteins.

Figure 6. TAC-1 and ZYG-9 Stabilize Each Other in *C. elegans* Embryos

(A–D) One-cell-stage embryos stained with antibodies against (A and B) ZYG-9 or (C and D) TAC-1, as well as against α-tubulin; wild-type (anaphase, [A]; telophase, [C]), *tac-1(RNAi)* (metaphase, [B]), or *zyg-9(RNAi)* (telophase, [D]). The panels on the left show anti-ZYG-9 or anti-TAC-1 staining, and the panels on the right show a merge of ZYG-9 or TAC-1 (red), α-tubulin (green), and Hoechst counterstain to view DNA (blue). Both centrosomal and cytoplasmic ZYG-9 is diminished in *tac-1(RNAi)* embryos (compare [A] and [B]), as is the case for TAC-1 in *zyg-9(RNAi)* embryos (compare [C] and [D]).

(E) Western blot analysis of wild-type, *tac-1(RNAi)*, and *zyg-9(RNAi)* embryonic extracts probed with anti-ZYG-9 and reprobed with anti-TAC-1 and anti-α-tubulin antibodies. Using the α-tubulin signal to normalize the concentration of each extract, we estimate that ~10% of the wild-type levels of TAC-1 are left in *zyg-9(RNAi)* embryos and, conversely, that ~10% of the wild-type levels of ZYG-9 are left in *tac-1(RNAi)* embryos.

(F–G) (F) A wild-type or (G) weak *tac-1(RNAi)* prometaphase one-cell-stage embryo probed with anti-ZYG-9 and anti-α-tubulin revealed by secondary antibodies as well as directly labeled TAC-1 antibodies. The merge shows ZYG-9 (red) and α-tubulin (green), as well as Hoechst counterstain to view DNA (blue). Note that while the level of centrosomal ZYG-9 is indistinguishable in wild-type and *tac-1(RNAi)* embryos, there is markedly less ZYG-9 in the cytoplasm when *tac-1* function is reduced.

We observed that TAC-1 distribution at centrosomes is not affected by the absence of microtubules, indicating that microtubules do not modulate the kinetics of binding or the release of TAC-1 from centrosomes. What, then, regulates this rapid exchange? One possibility is suggested by the observation that centrosomal TAC-1 is markedly diminished in embryos lacking the function of γ-tubulin and the Aurora-A kinase AIR-1. *Drosophila* Aurora-A kinase associates with and phosphorylates D-TACC and is also required for its centrosomal enrichment [27]. Because Aurora-A kinase also associates with Hs-TACC3 [27], it is probable that phosphorylation targets residues within the TACC domain that are likely to be conserved in TAC-1. One intriguing possibility is that Aurora-A kinase and γ-tubulin regulate centrosomal TACC protein distribution by modifying their rate of exchange with the cytoplasmic pool during centrosome maturation.

TAC-1 and ZYG-9 Form a Complex

TACC proteins interact with members of the evolutionarily conserved XMAP215 family of MAPs. Thus, D-TACC interacts with Msps, while Hs-TACC1 interacts with ch-TOG [12, 28]. However, the domains within these protein pairs that mediate binding have yet to be defined. In *C. elegans*, we found that TAC-1 efficiently binds ZYG-9, both in vitro and in vivo. Because TAC-1 essentially contains a TACC domain, it is likely that this is the protein region that mediates binding to XMAP215 family members across evolution. Reciprocally, we identified at least three regions within the C-terminal half of ZYG-9 that can mediate binding to TAC-1. Although this part of ZYG-9 is poorly conserved, we note that the C-terminal half of ch-TOG mediates interaction with Hs-TACC1 [28], while that of XMAP215 directs centrosomal targeting [29]. These findings suggest that it may also mediate binding to Maskin.

Our findings indicate that the bulk of TAC-1 and ZYG-9 is present in a complex in *C. elegans* embryos. In contrast, it appears that not all of D-TACC or Msps is present in the D-TACC/Msp complex in *Drosophila* embryos [12, 13]. It could be that regions outside the TACC domain engage D-TACC in interactions with other partners that could not take place in the case of the shorter TAC-1.

TAC-1 and ZYG-9 Stabilize Each Other

A prevailing model to explain how D-TACC and Msps promote microtubule assembly posits that D-TACC recruits Msps to centrosomes, thus ensuring that Msps can bind to and stabilize microtubule plus ends as they grow [12]. A prediction of this model is that while Msps localization at centrosomes requires *d-tacc* function, D-TACC localization at centrosomes may be independent of *msps* function. Indeed, centrosomal Msps is lost in *d-tacc* mutants, whereas centrosomal D-TACC is not affected in *msps* mutants, although substantial residual protein (~10%–20%) is produced in the *msps* mutants utilized in these experiments [13]. In *C. elegans*, by contrast, strong inactivation of either *tac-1* or *zyg-9* dramatically reduces centrosomal accumulation of the other interacting partner. Importantly, this reduction is not limited to the centrosome, but it occurs also in the cytoplasm, as shown both by immunofluorescence and Western blot analysis. Therefore, *tac-1* and *zyg-9* stabilize each other in *C. elegans*, and it will be interesting to test whether a similar situation holds for *Drosophila* when *msps* is inactivated in full.

The discovery of this mutual stabilization mechanism has important implications for the interpretation of the consequences of inactivating either component. For instance, our findings establishing that embryos lacking *tac-1* function have defects in microtubule assembly must be revisited and understood as a combined loss of *tac-1* and *zyg-9* function. Compatible with this view, we observed similar defects in microtubule assembly by using our FRAP-based assay after *zyg-9* inactivation (unpublished data). The molecular basis for the mutual stabilization is not known at present, although regulation at the level of protein stability seems most plausible given the tight interaction between TAC-1 and ZYG-9.

A Function for the TAC-1/ZYG-9 Complex in the Cytoplasm?

Although TACC proteins have been thought of as acting at centrosomes, our findings raise a distinct possibility. Unexpectedly, we found that rare *tac-1(RNAi)* embryos that exhibit a phenotype have diminished levels of ZYG-9 in the cytoplasm, but not at centrosomes. This finding indicates that normal amounts of centrosomal ZYG-9 are not sufficient for proper cell division. At least two possibilities could explain this observation. First, ZYG-9 may indeed be active at centrosomes but may require another function of *tac-1* that is distinct from that required for stabilization. For instance, TAC-1 could be needed for recruiting a putative positive regulator of ZYG-9. A second possibility is that ZYG-9 may be active primarily in the cytoplasm, where it would be ideally located to regulate microtubule plus end dynamics throughout the cell. Careful analysis of the regulation of the TAC-1/ZYG-9 complex will help to distinguish between these hypotheses and enhance our understanding of how modulation of microtubule dynamics contributes to cell division control.

Experimental Procedures

Nematode Strains

C. elegans (N2) culture was performed according to standard methods [30]. Homozygous mutant animals of the genotypes *spd-5(or-213ts)* [19] or *tbg-1(t1465)* [21] were grown at 15°C and were shifted to 24°C for 24 hr before analysis. Transgenic animals expressing GFP-β-tubulin and GFP-histone2B have been described [31]. For generation of GFP-TAC-1 transgenic animals, the *tac-1* coding sequence was subcloned from the pPC86 two-hybrid vector into pSU25, a modified version of the *pie1-gfp* vector containing the *unc-119* cDNA (a gift from Michael Glotzer). The sequence-verified construct was bombarded by following established procedures [31], and an integrated GFP-TAC-1 line was recovered.

RNAi

tac-1(RNAi) was performed initially by microinjection of dsRNA; we then generated an RNAi feeding strain corresponding to full-length *tac-1* essentially as described [32]. The DIC microscopy phenotype resulting from *tac-1* inactivation by either method was identical, and the feeding strain, feeding >24 hr at 20°C, was utilized for all experiments illustrated in the manuscript. Briefer (~12 hr) exposure to dsRNA resulted in a milder phenotype in which migration of pronuclei took place but subsequent centration/rotation failed.

Other feeding strains were generated in a similar manner, and animals were fed as follows: *dhc-1(RNAi)* (a gift from Moira Cockell), 30 hr at 20°C; *tba-2(RNAi)* (a gift from Michael Glotzer), 24 hr at 24°C; and *air-1(RNAi)* (a gift from Rémi Sonneville), 45 hr at 20°C.

Time-Lapse Microscopy

Wide-field dual DIC and fluorescent time-lapse microscopy were performed as described [33]; one image pair was captured every 10 s. Pole-to-pole distances were measured during metaphase and late anaphase in ten wild-type DIC movies and ten *tac-1(RNAi)* DIC movies by using Scion Image software.

Spinning-disc time-lapse confocal microscopy was conducted with a 63× N.A. 1.4 Apochromat lens on a Zeiss Axiovert 200 microscope equipped with a HQ monochrome CCD camera (Roper Scientific) with a 488 nm laser (Laser Physic, 1% laser power) and a Yokagawa scan head (VisiTech International); one image was captured every 5 s.

FRAP experiments were performed with a 63× N.A. 1.4 Apochromat lens on a LSM510 Zeiss confocal microscope, which photobleached a region of interest with 50 iterations and 100% laser power. For GFP-TUB, a single ~1 μm confocal slice was acquired at each time point. Recovery of fluorescence was monitored in two areas: a ~3–4 μm^2 square corresponding to the bleached area, and a disc ~2 μm in diameter corresponding strictly to the centrosome. We susbtracted the values obtained in the disc, which reflect both nucleation and growth rates, from those obtained in the square to focus the analysis on overall assembly rates. We defined the initial recovery speed (IRS) between the two first time points of recovery as a kinetic parameter most appropriately reflecting growth rates shortly after photobleaching. For GFP-TAC-1, seven ~1 μm confocal slices were acquired at each time point, and fluorescence recovery was monitored in the full projection within the bleached area and within the other centrosome as an internal control.

Anti-TAC-1 Antibodies

Full-length *tac-1* cDNA was subcloned into pGEX-6P (Pharmacia). GST-TAC-1 fusion protein was produced, purified, and digested with PreScission protease. TAC-1 was then injected into a rabbit according to standard procedures (Eurogentec). Anti-TAC-1 antibodies were affinity purified by using a Hitrap NHS column (Amersham Pharmacia) coupled to the antigen and were stored at 0.2 mg/ml.

Direct labeling of affinity-purified antibodies with Cy5 was performed by using the Maleimide Mono-Reactive Dye 5-Pack (Pharmacia).

Immunofluorescence

Fixation and indirect immunofluorescence were performed essentially as described [17], except that directly labeled anti-TAC-1 antibodies were incubated for 45 min at room temperature after incubation with the secondary antibodies. Microtubule depolymerization was achieved by placing the slide for 20 min on an aluminum block precooled on ice prior to fixation.

The primary antibodies used were 1:400 mouse anti-tubulin (DM1α; Sigma), 1:6000 rabbit anti-ZYG-9, and 1:200 rabbit anti-TAC-1. The secondary antibodies used were 1:2000 goat anti-mouse Alexa488 (Molecular Probes) and 1:2000 donkey anti-rabbit Cy3 (Dianova). Slides were counterstained with Hoechst 33258 (Sigma) to reveal DNA. All immunofluorescence data are represented as single 0.7–0.8 μm thick confocal slices. Images were processed with Adobe Photoshop; relative signal intensities were preserved.

Immunoprecipitation

Immunoprecipitations (Ips) were performed on worm embryonic extracts prepared from ~1.5 ml pelleted embryos. Embryos were resuspended in 1.5 ml Ip buffer (100 mM HEPES, 750 mM NaCl, 10 mM $MgCl_2$, 50 mM EDTA, 1 mM DTT, protease inhibitors [cocktail P8340 from Sigma, diluted 1:1000]) and snap frozen in liquid nitrogen. A powder was collected by grinding frozen material with a pestle in a ceramic bowl. The material was then thawed on ice, and the soluble fraction was separated from lipids and debris by centrifugation (15,000 × g, 10 min at 4°C) prior to preclearing on proteinG-sepharose beads for 30 min at 4°C. A fraction of the extract was kept for analysis, and the remaining volume was split in three for anti-TAC-1, anti-ZYG-9, and anti-GFP (a gift from Viesturs Simanis) Ip. Antibodies (5 μg/ml final concentration) were incubated with extract for 2 hr at 4°C. ProteinG-sepharose was then added for 1 hr to immobilize immunocomplexes. The flow-through fractions were kept for analysis, and beads were washed once with Ip buffer and twice with PBS prior to Western blot analysis (see the Supplemental Data).

Supplemental Data

Supplemental Data including additional Experimental Procedures, two figures, and three movies can be found at http://www.current-biology.com/cgi/content/full/13/17/1488/DC1/.

Acknowledgments

We are grateful to Anne Debant, Marie Delattre, and Viesturs Simanis for critical reading of the manuscript, to Bruce Bowerman, Moira Cockell, Michael Glotzer, Viesturs Simanis, and Rémi Sonneville for reagents, as well as to Karine Baumer for technical assistance. This work was supported by an European Molecular Biology Organization long-term fellowship (ALTF 497-2001 to J.-M.B.) and a grant from the Swiss National Science Foundation (31-62102.00 to P.G.).

Received: July 1, 2003
Revised: July 22, 2003
Accepted: July 23, 2003
Published: September 2, 2003

References

1. Mitchison, T.J., and Kirschner, T.J. (1984). Dynamic instability of microtubule growth. Nature *312*, 237–242.
2. Holy, T.E., and Leibler, S. (1994). Dynamic instability of microtubules as an efficient way to search in space. Proc. Natl. Acad. Sci. USA *91*, 5682–5685.
3. Gard, D.L., and Kirschner, M.W. (1987). A microtubule-associated protein from *Xenopus* eggs that specifically promotes assembly at the plus-end. J. Cell Biol. *105*, 2203–2215.
4. Vasquez, R.J., Gard, D.L., and Cassimeris, L. (1994). XMAP from *Xenopus* eggs promotes rapid plus end assembly of microtubules and rapid microtubule polymer turnover. J. Cell Biol. *127*, 985–993.
5. Kinoshita, K., Arnal, I., Desai, A., Drechsel, D.N., and Hyman, A.A. (2001). Reconstitution of physiological microtubule dynamics using purified components. Science *294*, 1340–1343.
6. Kinoshita, K., Habermann, B., and Hyman, A.A. (2002). XMAP215: a key component of the dynamic microtubule cytoskeleton. Trends Cell Biol. *12*, 267–273.
7. Kemphues, K.J., Wolf, N., Wood, W.B., and Hirsh, D. (1986). Two loci required for cytoplasmic organization in early embryos of *Caenorhabditis elegans*. Dev. Biol. *113*, 449–460.
8. Kosco, K.A., Pearson, C.G., Maddox, P.S., Wang, P.J., Adams, I.R., Salmon, E.D., Bloom, K., and Huffaker, T.C. (2001). Control of microtubule dynamics by Stu2p is essential for spindle orientation and metaphase chromosome alignment in yeast. Mol. Biol. Cell *12*, 2870–2880.
9. Whittington, A.T., Vugrek, O., Wei, K.J., Hasenbein, N.G., Sugimoto, K., Rashbrooke, M.C., and Wasteneys, G.O. (2001). MOR1 is essential for organizing cortical microtubules in plants. Nature *411*, 610–613.
10. Cullen, C.F., Deak, P., Glover, D.M., and Ohkura, H. (1999). mini spindles: a gene encoding a conserved microtubule-associated protein required for the integrity of the mitotic spindle in *Drosophila*. J. Cell Biol. *146*, 1005–1018.
11. Shirasu-Hiza, M., Coughlin, P., and Mitchison, T. (2003). Identification of XMAP215 as a microtubule-destabilizing factor in *Xenopus* egg extract by biochemical purification. J. Cell Biol. *161*, 349–358.
12. Lee, M.J., Gergely, F., Jeffers, K., Peak-Chew, S.Y., and Raff, J.W. (2001). Msps/XMAP215 interacts with the centrosomal protein D-TACC to regulate microtubule behaviour. Nat. Cell Biol. *3*, 643–649.

13. Cullen, C.F., and Ohkura, H. (2001). Msps protein is localized to acentrosomal poles to ensure bipolarity of *Drosophila* meiotic spindles. Nat. Cell Biol. *3*, 637–642.
14. Matthews, L.R., Carter, P., Thierry, M.D., and Kemphues, K. (1998). ZYG-9, a *Caenorhabditis elegans* protein required for microtubule organization and function, is a component of meiotic and mitotic spindle poles. J. Cell Biol. *141*, 1159–1168.
15. Gönczy, P., Bellanger, J.M., Kirkham, M., Pozniakowski, A., Baumer, K., Phillips, J.B., and Hyman, A.A. (2001). *zyg-8*, a gene required for spindle positioning in *C. elegans*, encodes a doublecortin-related kinase that promotes microtubule assembly. Dev. Cell *1*, 363–375.
16. Gergely, F. (2002). Centrosomal TACCtics. Bioessays *24*, 915–925.
17. Gönczy, P., Schnabel, H., Kaletta, T., Amores, A.D., Hyman, T., and Schnabel, R. (1999). Dissection of cell division processes in the one cell stage *Caenorhabditis elegans* embryo by mutational analysis. J. Cell Biol. *144*, 927–946.
18. Gönczy, P., Pichler, S., Kirkham, M., and Hyman, A.A. (1999). Cytoplasmic dynein is required for distinct aspects of MTOC positioning, including centrosome separation, in the one cell stage *Caenorhabditis elegans* embryo. J. Cell Biol. *147*, 135–150.
19. Hamill, D.R., Severson, A.F., Carter, J.C., and Bowerman, B. (2002). Centrosome maturation and mitotic spindle assembly in *C. elegans* require SPD-5, a protein with multiple coiled-coil domains. Dev. Cell *3*, 673–684.
20. Hannak, E., Kirkham, M., Hyman, A.A., and Oegema, K. (2001). Aurora-A kinase is required for centrosome maturation in *Caenorhabditis elegans*. J. Cell Biol. *155*, 1109–1116.
21. Hannak, E., Oegema, K., Kirkham, M., Gönczy, P., Habermann, B., and Hyman, A.A. (2002). The kinetically dominant assembly pathway for centrosomal asters in *Caenorhabditis elegans* is gamma-tubulin dependent. J. Cell Biol. *157*, 591–602.
22. Strome, S., Powers, J., Dunn, M., Reese, K., Malone, C.J., White, J., Seydoux, G., and Saxton, W. (2001). Spindle dynamics and the role of gamma-tubulin in early *Caenorhabditis elegans* embryos. Mol. Biol. Cell *12*, 1751–1764.
23. Raff, J.W. (2002). Centrosomes and cancer: lessons from a TACC. Trends Cell Biol. *12*, 222–225.
24. Gergely, F., Kidd, D., Jeffers, K., Wakefield, J.G., and Raff, J.W. (2000). D-TACC: a novel centrosomal protein required for normal spindle function in the early *Drosophila* embryo. EMBO J. *19*, 241–252.
25. Gergely, F., Karlsson, C., Still, I., Cowell, J., Kilmartin, J., and Raff, J.W. (2000). The TACC domain identifies a family of centrosomal proteins that can interact with microtubules. Proc. Natl. Acad. Sci. USA *97*, 14352–14357.
26. Raff, J.W., Jeffers, K., and Huang, J.Y. (2002). The roles of Fzy/Cdc20 and Fzr/Cdh1 in regulating the destruction of cyclin B in space and time. J. Cell Biol. *157*, 1139–1149.
27. Giet, R., McLean, D., Descamps, S., Lee, M.J., Raff, J.W., Prigent, C., and Glover, D.M. (2002). *Drosophila* Aurora A kinase is required to localize D-TACC to centrosomes and to regulate astral microtubules. J. Cell Biol. *156*, 437–451.
28. Lauffart, B., Howell, S.J., Tasch, J.E., Cowell, J.K., and Still, I.H. (2002). Interaction of the transforming acidic coiled-coil 1 (TACC1) protein with ch-TOG and GAS41/NuBI1 suggests multiple TACC1-containing protein complexes in human cells. Biochem. J. *363*, 195–200.
29. Popov, A.V., Pozniakovsky, A., Arnal, I., Antony, C., Ashford, A.J., Kinoshita, K., Tournebize, R., Hyman, A.A., and Karsenti, E. (2001). XMAP215 regulates microtubule dynamics through two distinct domains. EMBO J. *20*, 397–410.
30. Brenner, S. (1974). The genetics of *Caenorhabditis elegans*. Genetics *77*, 71–94.
31. Praitis, V., Casey, E., Collar, D., and Austin, J. (2001). Creation of low-copy integrated transgenic lines in *Caenorhabditis elegans*. Genetics *157*, 1217–1226.
32. Timmons, L., Court, D.L., and Fire, A. (2001). Ingestion of bacterially expressed dsRNAs can produce specific and potent genetic interference in *Caenorhabditis elegans*. Gene *263*, 103–112.
33. Brauchle, M., Baumer, K., and Gönczy, P. (2003). Differential activation of the DNA replication checkpoint contributes to asynchrony of cell division in *C. elegans* embryos. Curr. Biol. *13*, 819–827.